Nanoscale

PAPER

View Article Online
View Journal | View Issue

Cite this: *Nanoscale*, 2017, **9**, 10897

Laser-engraved carbon nanotube paper for instilling high sensitivity, high stretchability, and high linearity in strain sensors†

Yangyang Xin, Jian Zhou,* Xuezhu Xu and Gilles Lubineau *

Received 6th March 2017,
Accepted 19th June 2017

DOI: 10.1039/c7nr01626c

rsc.li/nanoscale

There is an increasing demand for strain sensors with high sensitivity and high stretchability for new applications such as robotics or wearable electronics. However, for the available technologies, the sensitivity of the sensors varies widely. These sensors are also highly nonlinear, making reliable measurement challenging. Here we introduce a new family of sensors composed of a laser-engraved carbon nanotube paper embedded in an elastomer. A roll-to-roll pressing of these sensors activates a pre-defined fragmentation process, which results in a well-controlled, fragmented microstructure. Such sensors are reproducible and durable and can attain ultrahigh sensitivity and high stretchability (with a gauge factor of over 4.2×10^4 at 150% strain). Moreover, they can attain high linearity from 0% to 15% and from 22% to 150% strain. They are good candidates for stretchable electronic applications that require high sensitivity and linearity at large strains.

1. Introduction

With the rapid development of stretchable electronic devices, stretchable conductive materials have continued to receive considerable attention, as they bring new possibilities for achieving both conductivity and stretchability.[1–7] Conventional strain sensors, like metallic gauges, have evolved towards high stretchability to adapt to the emerging applications like wearable electronics, artificial e-skins, and bionic sensory systems.[1,8–17] For instance, highly stretchable strain sensors play a vital role in the construction of artificial sensory systems for human movement detection and touch sensing.[3,18–20] The main factors that determine the performance of a strain sensor are sensitivity, stretchability, and linearity. The sensitivity, represented by the gauge factor (GF), is evaluated by the relative resistance change *versus* the applied strain. High GF sensors are vital for small strain detection and open up opportunities for the exploration of subtle strain detection. Stretchability is the maximum uniaxial tensile strain of the sensor before failure, which determines the sensing strain range. The linearity is significant for stretchable strain sensors because nonlinearity makes the calibration process difficult. However, conventional strain sensors cannot achieve a satisfactory combination of high sensitivity (GF >100), high stretchability (strain >100%), and high linearity. This limits the development of applications in wearable electronics.

One of the most effective ways to impart stretchability to highly conductive and brittle materials is the formation of cracks in the material on stretchable substrates.[1] In fact, devices do not necessarily fail at the point when the active materials crack from stretching.[21,22] The formation of cracks on metallic films has been a useful technique for creating stretchable metallic conductors. For example, strain sensors made of cracked silver nanoparticle (AgNP) thin films coated on polydimethylsiloxane (PDMS) substrates can be stretched up to 20% with GF = 7. The change in resistance is attributed to the opening and closing of microcracks.[23] Strain sensors with ultrahigh sensitivity (GF >2000) have been reported based on the formation of nano cracks in a platinum thin film deposited on top of stretchable layers; yet, while their GF could reach 16 000 by engineering the crack depth, their stretchability was limited to just 2%.[24] The sensing mechanism of this nano crack based sensor is ascribed to a disconnection–reconnection process undergone by nanoscale crack junctions under strain or vibration.[24–26] Although these examples cannot achieve high stretchability, they have motivated scientists to develop new materials and structures that can endure large mechanical deformations. By generating microcracks in the thickness gradient of a carbon nanotube (CNT) film, strain sensing could be larger than 100% of the strain. However, the GFs of the sensor decreased from 161 to 0.58 when it was

King Abdullah University of Science and Technology (KAUST), Physical Sciences and Engineering Division, COHMAS Laboratory, Thuwal 23955-6900, Saudi Arabia.
E-mail: jian.zhou@kaust.edu.sa, gilles.lubineau@kaust.edu.sa;
Tel: +966(12)8082983

†Electronic supplementary information (ESI) available. See DOI: 10.1039/C7NR01626C

stretched to 15%, showing large sensitivity deviations in the strain measurement range.[27] Sensors made of graphite thin films with short microcracks possess high GF (a maximum value of 522.6) and stretchability ($\varepsilon \geq 50\%$), whereas sensors with long microcracks show ultrahigh sensitivity (a maximum value of 11 344) with limited stretchability ($\varepsilon \leq 50\%$).[28] In our previous study, we have demonstrated that fragmented single-walled carbon nanotube (SWCNT) paper in PDMS functioned as an ultrasensitive and stretchable strain sensor. Our approach suggests a path towards the formation of fragmented SWCNT paper sensors with a high GF of 10^7 at a maximum strain of 50%. However, due to the high stress concentration at the cracked paper/PDMS interface, the PDMS substrate experiences an early mechanical failure after 50%. This will limit the lifetime of the sensor at higher strains.[12] The results show a paradox: achieving high sensitivity requires a large deformation of the microstructure upon stretching. Yet, achieving high stretchability requires minimizing the effect of microstructure defects induced by stress concentration, so that the integrity of the microstructure is preserved at large strains. As a result, both characteristics could not be obtained simultaneously in simple thin film structures. We show here that this paradox can be overcome by using a well-controlled network of cracks.

Here, we introduce a new strategy to construct high-performance strain sensors with laser-engraved SWCNT papers. We first introduce surface cracks with controlled density into SWCNT papers using a laser-engraving process. Then the laser-engraved SWCNT paper is embedded in the PDMS substrate, followed by a roll-to-roll pressing process to trigger crack formation. A dense network of cracks (3.3 mm^{-1}) in the sensor allows us to obtain a maximum stretchability of 153% while maintaining a high sensitivity of 4.2×10^4. Moreover, the dense and well-controlled network of cracks enables a high linearity of the sensing response. The combination of high sensitivity, high stretchability, and high linearity of the sensor will be vital for the development of stretchable electronics.

2. Experimental

2.1 Materials

SWCNTs with 2.7% COOH groups were purchased from CheapTubes, Inc., with over 90 wt% purity and containing more than 5 wt% of multi-walled CNT. The SWCNT length ranged from 5 to 30 mm and their outer diameter ranged from 1 to 2 nm. The true density of these SWCNTs was 2.1 g cm^{-3}. SYLGARD 184 PDMS and methanesulfonic acid (CH_3SO_3H) were purchased from Sigma Aldrich.

2.2 Preparation of SWCNT paper

Preparation methods have been reported in a previous study.[12] An improved experimental procedure was performed as shown in Fig. S1.† An environmentally friendly mild organic acid, methanesulfonic acid (CH_3SO_3H), was used to disperse SWCNTs to increase the safety of handling the material (compared to superacids like chlorosulfonic acid).[29] A 0.5 wt% SWCNT dope was prepared by adding 0.2 g of SWCNTs into 40 g of CH_3SO_3H, sealing in a glass bottle, stirring for 5 min and bath sonicating using a Brason 8510 sonicator (250 W; Thomas Scientific) for 60 min. The mixture was then stirred again for 12 h at 500 rpm. 15 g of the 0.5% SWCNT/CH_3SO_3H dispersion were vacuum-filtered through a ceramic filtration membrane (pore size: 20 nm, Whatman).

In this vacuum-filtered process, the vacuum was about −0.86 bar. Any remaining CH_3SO_3H was removed from the sample by washing it with 200 mL of water. To remove the surface tension on the SWCNT paper, another polycarbonate (PC) filter (pore size: 50 nm, Whatman) was placed on top of the SWCNT paper, followed by a porous plastic disc (thickness 300 μm) placed on the PC filter. The vacuum was then pumped for an additional 5 hours. The free-standing SWCNT paper was then peeled off from the filter for the laser engraving. The thickness of the SWCNT paper, measured using a DML3032 digital thickness micrometer under a constant pressure of 6 kPa, was about 90 ± 5 μm.

2.3 Laser engraving on the SWCNT paper

High-density grooves were created using a PLS6MW-Multi-Wavelength Laser Platform and a 1.06 μm fiber laser source (Universal Laser Systems). The sample was cut with a power of 24 W at a speed of 160 cm s^{-1} and a frequency of 400 kHz to ensure a non-through-thickness channel, as shown in Fig. 1a. The pre-crack depth should be chosen as the minimum depth that is enough to trigger the crack initiation. Values more than the minimum depth would result in degraded functional properties due to the reduction of the effective thickness of the paper. The distance between the laser source and the SWCNT paper was controlled by setting the Z stepping motor at 2 mm. The average spacing between the cracks, D, was easily controlled at D = 2.0, 0.9, 0.6, 0.5, and 0.3 mm corresponding to different crack densities, $1/D$, of 0.5, 1.1, 1.7, 2.0 and 3.3 mm^{-1}. The laser-engraved SWCNT papers were then cut into 30 × 3 mm^2 strips for preparing the strain sensors (Fig. S3a†).

2.4 Preparation of SWCNT paper-based strain sensors

The strips of laser-engraved SWCNT paper were transferred onto 0.5 mm-thick PDMS substrates; copper wires were connected to the SWCNT paper strips by silver epoxy. Next, a second layer of PDMS precursor of equal weight was poured onto the sample and cured at 70 °C in an oven for 2 h to fully encapsulate the SWCNT paper.[12] To remove the air bubbles from the SWCNT strip and the PDMS before curing, we treated the sample in a vacuum oven with about −0.94 bar vacuum. Then the samples were cut using a laser cutting machine (Universal Laser Systems) with dimensions of 5 mm × 1 mm × 4 mm, and a 4 mm-diameter notch was cut into PDMS substrates (Fig. S3b†).

2.5 Initiation of through-thickness cracks by the roll-to-roll pressing method

The samples were loaded into a self-designed roll-to-roll pressing device as shown in Fig. 1d. Cracks were propagated

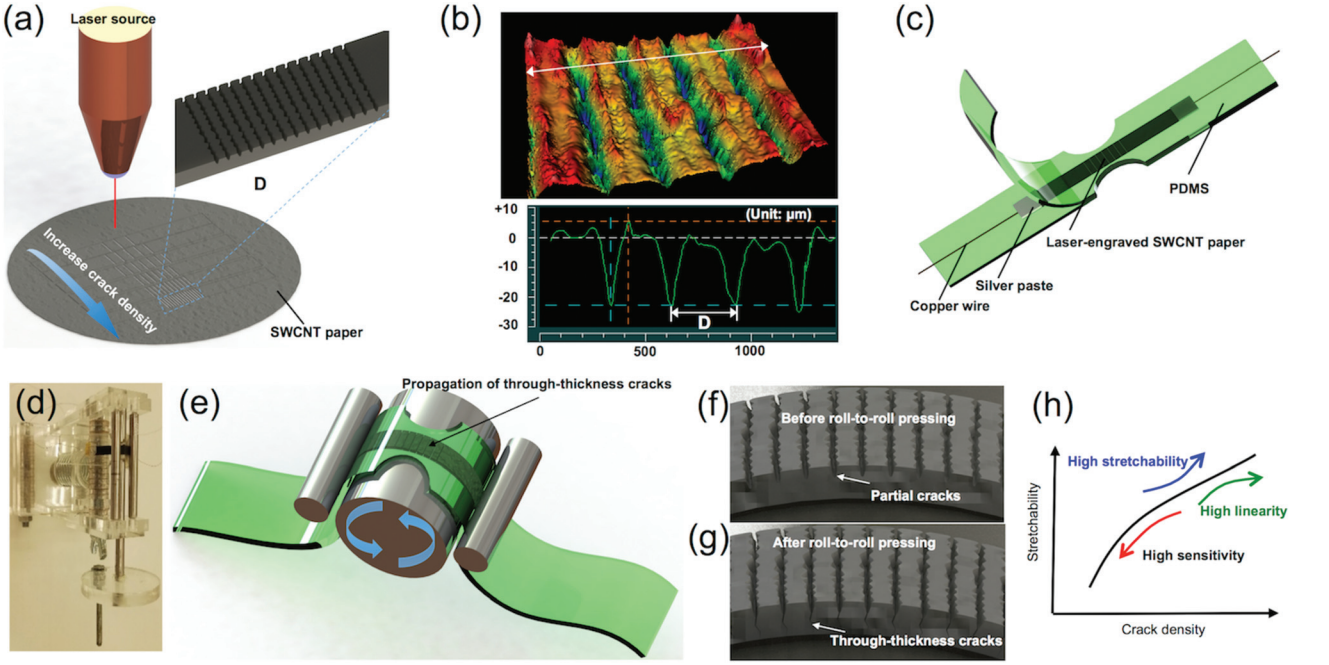

Fig. 1 Proposed strategy to control the crack density of the SWCNT paper in an elastomer for high sensitivity, high stretchability, and high linearity in strain sensors. (a) Illustration images present the laser-engraving process for generating partial cracks on the SWCNT paper. (b) 3D profiles and crack depth of the laser-engraved SWCNT paper measured by an optical profiler. *D* represents the average spacing between the cracks. (c) Illustration of a typical sample: the laser-engraved SWCNT paper embedded in the PDMS substrate. (d) and (e) Real and illustrated examples of a roll-to-roll pressing device for the propagation of through-thickness cracks in the SWCNT paper, respectively. (f) and (g) Graphs demonstrating the structure of the laser-engraved SWCNT paper before and after roll-to-roll pressing, respectively. Arrows in (f) and (g) show the partial and through-thickness cracks before and after roll-to-roll pressing, respectively. (h) The proposed strategy and structure would help achieve a combination of high sensitivity, high stretchability, and high linearity of the strain sensor.

through the whole thickness by pressing the sample in alternating clockwise and counterclockwise directions until all cracks were created (Fig. 1f and g).

2.6 Characterization

Scanning electron microscopy (SEM) on SWCNT paper was performed using a Quanta 3D (FEI Company). The surface morphology of the laser-engraved SWCNT paper was probed using a NewView 7100 profilometer (Zygo Corporation).

To avoid any sliding of the sample during stretching, poly (methyl methacrylate) (PMMA) grips with groove structures were fabricated by laser cutting, and the samples were glued to the grips by a PDMS precursor, and then cured (as shown in Fig. S3c†). The cyclic stretching and relaxing motion of the sample was controlled by using a 5944 Instron machine. The PMMA grips with samples were clamped by the Instron machine (Fig. S3d†). A 4 mm gap between the grips was equivalent to the length of the sample. The change in electrical resistance of the specimen was monitored using a U1252B digital multimeter. The incremental, cyclic stretching and relaxing program was applied to the sample to detect the maximum stretchability of the sensor. The program was set with an incremental strain of 25%, starting from 0% and continuing until the failure of the sample at a speed of 1.2 mm min^{-1}. To determine the average maximum stretchability of the sensor, at least five samples were tested at each crack density in the incremental cyclic program. The stretching and relaxing process of the SWCNT paper in PDMS was monitored by using a video camera. The gauge factor (GF) of the strain sensors was defined by GF = $(\Delta R/R_0)/\varepsilon$, where R_0 is the initial resistance, $\Delta R/R_0$ is the relative change in resistance, and ε is the applied strain.

For electrical impedance spectroscopy (EIS), the modulus of impedance, Z, and phase angle, θ, were acquired simultaneously with an Agilent E4980A Precision LCR meter in a two-probe configuration using Kelvin clips.[12,13] The frequency range spanned from 20 Hz to 2 MHz with a step of 1000 Hz and a sweep current of 50 mA. To understand the sensing mechanism in the cracked samples, we systematically investigated the change in impedance with frequency at different applied strains (0%, 5%, 30%, 50%, 75%, 100%, 125% and 150%).

3. Results and discussion

3.1 Controlled fragmentation of SWCNT papers

Fig. 1 shows the key concept and method of designing a stretchable strain sensor. The stretchability is dramatically improved by creating a high density of cracks containing conductive networks. Therefore, how to obtain SWCNT paper with

controlled crack density in an elastic substrate is a crucial point. First, SWCNT paper was prepared through vacuum filtration of 0.5 wt% SWCNT in methanesulfuric acid (CH_3SO_3H; for more details see the Experimental section and Fig. S1†). Fig. 1a shows that the laser-engraving process created partial cracks (partial meaning not penetrating through the whole thickness) on SWCNT paper. This approach is critical for controlling the location of the cracks and for maintaining the integrity and functionality of the SWCNT networks below the surface cracks. By decreasing the average spacing, D, between the cracks, the crack density, $1/D$, can be increased. Three dimensional mapping using an optical profilometer showed that the partial cracks had an average depth of 20 μm and an average spacing of 300 μm (Fig. 1b and Fig. S2, S3a†). Next, we embedded the laser-engraved SWCNT paper into a PDMS substrate (Fig. 1c). To avoid inhomogeneous crack generation, a roll-to-roll pressing process was repeatedly applied in clockwise and counterclockwise directions to fully complete the fragmentation of SWCNT papers, guided by the surface cracks as shown in Fig. 1e–g. Upon roll-to-roll pressing, cracks opened and penetrated through the thickness of the SWCNT paper. The average spacing, D, between the cracks was successfully controlled at 2.0, 0.9, 0.6, 0.5 and 0.3 mm at the corresponding crack densities, $1/D$, of 0.5, 1.1, 1.7, 2.0 and 3.3 mm^{-1}. These results prove that the laser engraving and roll-to-roll processes effectively control the cracking pattern. These through-thickness cracks are a key element for strain sensing. The crack-guided fragmentation in this study is superior to the previous method of stretching the SWCNT assembly, during which the crack spacing can only be coarsely controlled by engineering the thickness of the SWCNT paper.[12] It also has advantages over the previously reported metal nanofilm fragmentation, in which cracks were formed in an uncontrollable manner through bending deformation.[1,11] The ability to control the crack density in the SWCNT paper is a prerequisite for tuning the stretchability of the sensor. Moreover, at higher crack density, the microstructure of the cracks undergoes homogeneous propagation, which leads to an improved linear response of the strain sensor (Fig. 1h). The dense and well-controlled network of cracks contributes to high linearity.

Fig. 2a and Fig. S4† depict the evolution of the crack opening in a PDMS-embedded SWCNT paper with high crack density (3.3 mm^{-1}). As the sensor underwent stretching, the distributed cracks developed with their crack size correlated to the applied strain. These cracks acted as "switches", adjusting the density of the conductive networks of the sensor. The evolution of the average crack opening distance, L_c, with strain was almost linear (Fig. 2b), testifying to the overall linear elastic response of the sensor. As the strain ranged from 0% to 150%,

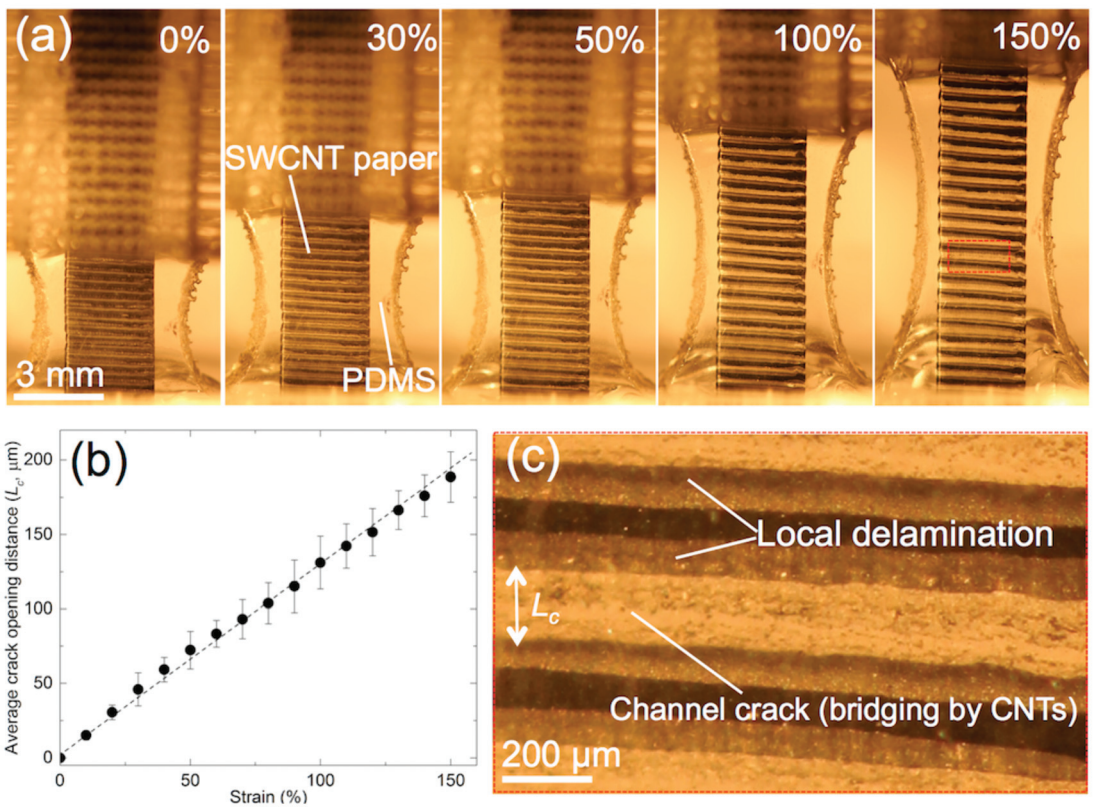

Fig. 2 Opening of cracks in a high crack density SWCNT paper (3.3 mm^{-1}) embedded in the PDMS substrate. (a) Images of a typical, high-crack-density SWCNT paper in PDMS when stretched from 0% to 150% strain. (b) Opening of cracks with the applied strain. (c) Channel crack and local decontaminations of the sample at 150% strain.

the resistance of the paper increased with applied strain from 15 Ω to 1.2 MΩ. As expected, samples with larger opening distances exhibited larger resistance under strain. Local delamination between the SWCNT paper and the PDMS substrate was clearly observed around crack edges because channel cracks cause severe out-of-plane stresses at the interfaces in the vicinity of the crack (Fig. 2c). SWCNT networks were also observed between the crack edges and play a key role of the sensing component during stretching.

3.2 Strain sensing

Fig. 3a presents the maximum stretchability, ε_m, of the sensor with different crack densities. The ε_m was increased from 60% to 153% by increasing the crack density from 0.5 to 3.33 mm^{-1}, indicating the working range of the sensors at various crack densities (Fig. 3a and Fig. S5†). This trend suggests that increasing the crack density in SWCNT paper dramatically increases the stretchability, proving that the prediction in Fig. 1h is reasonable. In a previous study, the stretchability of the SWCNT paper-based sensor was limited to 50–60% at low crack density ($1/D$ = 0.5 mm^{-1}) due to the high stress concentration around the cracks.[12] The stress concentration near the cracks was high enough to result in an early failure of the PDMS substrate. Moreover, the sensor was showing an obvious nonlinearity due to the previously uncontrolled and quasi-random network of cracks. However, by introducing high crack density ($1/D$ = 3.33 mm^{-1}) to the SWCNT paper through laser engraving and roll-to-roll pressing, the sensor attained a maximum stretchability of 153% and a high linearity (Fig. 3b).

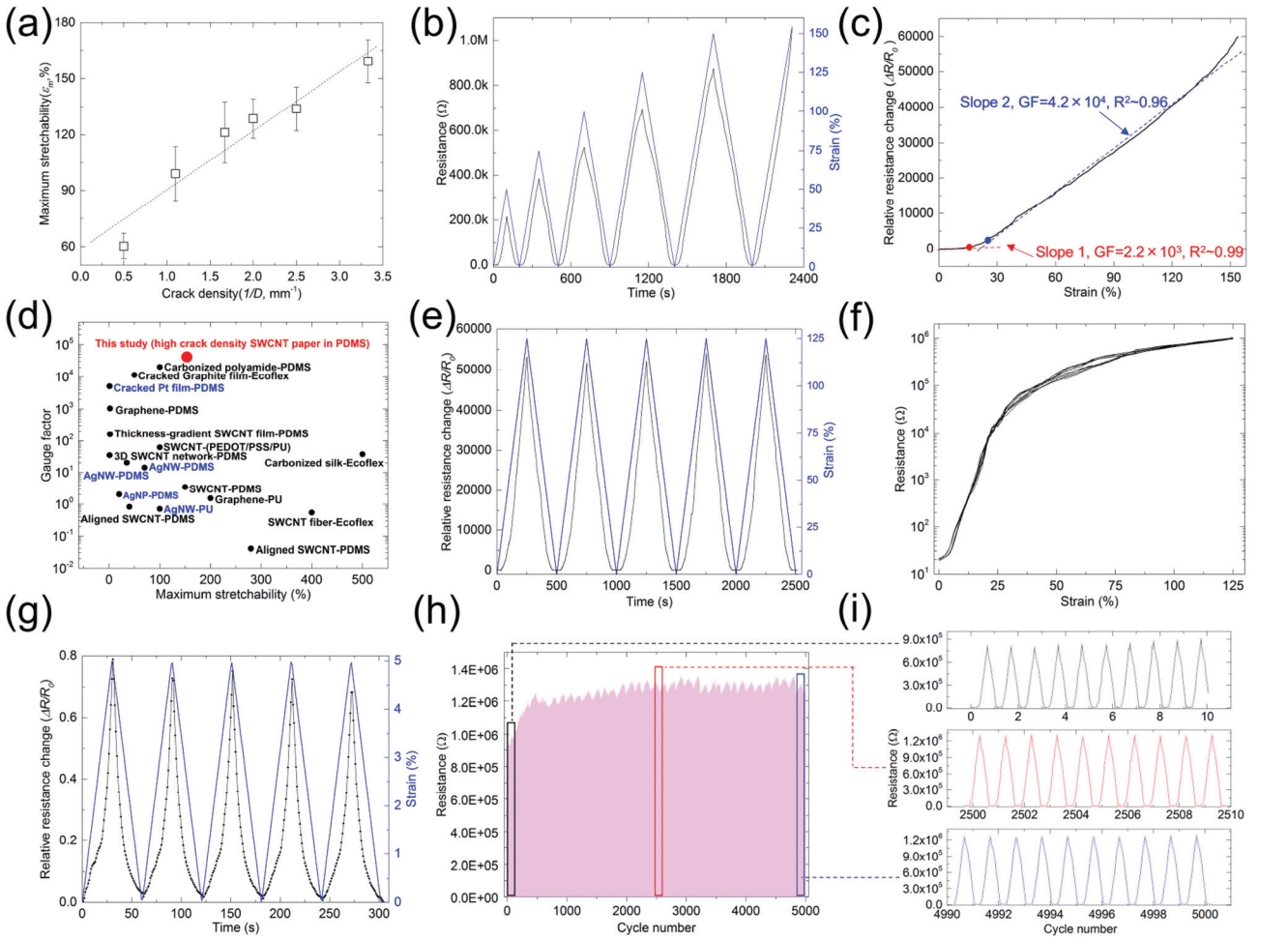

Fig. 3 High-crack-density SWCNT paper-based strain sensors. (a) The increase of the maximum stretchability of the sensors with crack density. (b) Resistance changes under incremental cyclic stretching and relaxing of a high-crack-density sensor ($1/D$ = 3.3 mm^{-1}). The maximum stretchability of the sensor is 153%. (c) Relative changes in resistance *versus* strain of the high-crack-density sensor ($1/D$ = 3.3 mm^{-1}). Red and blue dashed lines are the fitting slopes for strain from 0% to 15% with a linearity of 0.98 and strain from 22% to 150% with a linearity of 0.96, respectively. (d) GFs as a function of the maximum stretchability of recently reported conductive nanomaterial-based strain sensors.[1,27,30–36] (e) Dynamic response of the strain sensors to five stretching and relaxing cycles at 125%. (f) The curve of resistance changes against strain, showing extremely low hysteresis error of the sensor in (e). (g) Dynamic response of the strain sensors to stretching and relaxing cycles at 5%. (h) Dynamic response of the strain sensors to stretching/relaxing cycles at 80% at a speed of 6.4 mm min^{-1}, showing excellent long-term repeatability of the sensor. (i) Repeatability of the sensor at cycles 1 to 10, 2500 to 2510 and 4990 to 5000, as indicated in (h).

We plot the relative change in resistance ($\Delta R/R_0$) against strain for the sample with the highest stretchability in Fig. 3c. The change in resistance of this high crack-density SWCNT paper in PDMS is $\Delta R/R_0 = 6.1 \times 10^4$ at 150%. The sensing behavior of the sample is characterized by two linear regions with 2 different slopes (strain from 0% to 15% with a linearity of 0.98 and strain from 22% to 150% with a linearity of 0.96), which reflects the GF at different strain ranges: the GF was 2.2×10^3 (0% to 15%) and 4.2×10^4 (22% to 150%). In comparison, conventional metal gauges have a GF of around 2.0 at low strain ($\varepsilon < 5\%$).[1,2] The values of both GF and maximum stretchability are high compared with the performance of metal nanomaterial-based stretchable sensors.[24,37,38] Moreover, the GF of about 150% of our sample is the highest compared with recently reported values for stretchable strain sensors based on CNTs and graphene (Fig. 3d, Table S1†).[1,27,30–36] The results indicate that it could be used as an ultrasensitive strain sensor to detect the subtle change in strain with a wide strain detection range.

We also tested the dynamic durability of the sensor when exposed to cyclic stretching and relaxing. Fig. 3e presents five cycles of a strain from 0% to 125%, in which the $\Delta R/R_0$ evolved in a very reversible and stable manner, following the evolution of the applied strain closely. The reversibility becomes more obvious when we plot the resistance change against applied strain (Fig. 3f). The stretching and relaxing cycles almost overlap during each cycle, suggesting an extremely low hysteresis error. Note that delamination between the SWCNT paper and the PDMS substrate when stretching indicates a weak interfacial adhesion.[12] Dynamic durability can also be achieved at lower strain levels (5% tensile strain, Fig. 3g); the detection limit of the sensor was determined by applying an extremely low loading speed of 0.05 μm s^{-1}. Thanks to the high sensitivity of the sensor, the relative resistance change at a straining step of 0.001% was detectable, as shown in the inset of Fig. S6.† The effect of through-thickness cracks on the electrical resistance was clear at large strains and recoverable when the sample was released, indicating that the crack edges reconnect through SWCNT networks. After 5000 cycles of stretching and relaxing at 80% strain, the resistance of the strain sensor remained nearly unchanged (Fig. 3h and i). Resistance-type strain sensors often reach high GF or high stretchability, but normally with high hysteresis and nonlinearity.[1] The strain sensor based on high crack-density SWCNT papers displayed outstanding performance, combining high sensitivity, high stretchability, and high linearity. In summary, the high crack density led to several outcomes which resulted in high performance of the sensor: (1) the

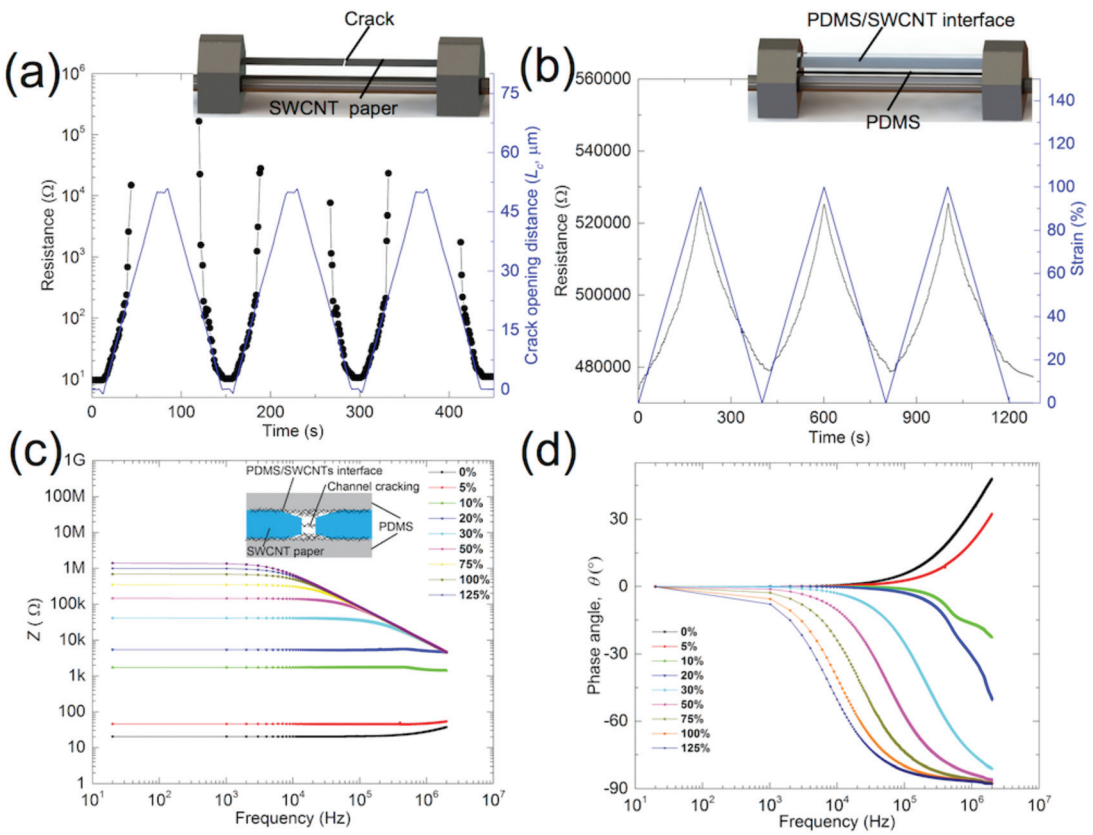

Fig. 4 Sensing mechanism. (a) and (b) Resistance changes under cyclic stretching and relaxing of a pure SWCNT paper and a PDMS/SWCNT interface, respectively. Insets in (a) and (b) show the illustrations of an SWCNT paper and an SWCNT interface on PDMS under loading, respectively. (c) and (d) Frequency dependence of the modulus of the complex impedance (Z) and phase angle (θ), respectively, of the SWCNT paper in PDMS. The inset in (c) shows the configuration of the sensor.

stress concentration near the crack was largely reduced by the large number of cracks; (2) stretchability was dramatically increased; (3) the dense and well-controlled network of cracks contributed to the high linearity.

3.3 Sensing mechanism

To investigate the sensing mechanism, we measure the change in resistance of a pure SWCNT paper and a PDMS/SWCNT interface separately with the applied strain. Fig. 4a shows the resistance change of a pure SWCNT paper with a single crack. A bending motion is applied to the paper to initiate a complete through-thickness crack (Fig. S7a†). Then dynamic stretching and relaxing are applied at a low speed of 0.12 mm min^{-1}. Fig. 4a shows the resistance recoverability of the paper for 3 cycles. A complete electrical disconnection occurs at 30 μm, indicating the critical connection distance of one crack in the SWCNT paper. The electrical disconnection distance lies in the length range of SWCNTs (5 to 30 μm). This also indicates that PDMS substrates are important for the resistance recovery of the SWCNT/PDMS sensor after relaxation. On the other hand, the upper PDMS layer was peeled off from the cracked SWCNT paper, revealing an opaque color and obvious CNT fragments are left on the interfacial layer (Fig. S7b†). This is consistent with a previous study suggesting that the PDMS precursor could infiltrate the SWCNT paper to some extent during the encapsulation.[12] It shows that the resistance of the interface increases almost linearly from 475 to 525 kΩ as the strain increases from 0% to 100%.

To explain the sensing mechanism of the sensors, we first performed a full characterization study of the impedance response over a wide range of frequencies, applied to the sensor made from the laser-engraved SWCNT paper embedded in PDMS. Fig. 4c and d show the frequency dependence of the modulus of the complex impedance (Z) and phase angle (θ), respectively. At low strains (ε < 20%), the impedance is nearly constant and the conduction mechanism is dominated by the resistive behavior of the SWCNT paper. Direct contact between CNTs at the crack region ensures macroscopic ohmic behavior. However, at higher strains (ε > 20%), the modulus of the complex impedance becomes considerably more frequency dependent. As the strain continues to increase, the SWCNTs become increasingly separated and disconnected. Conduction

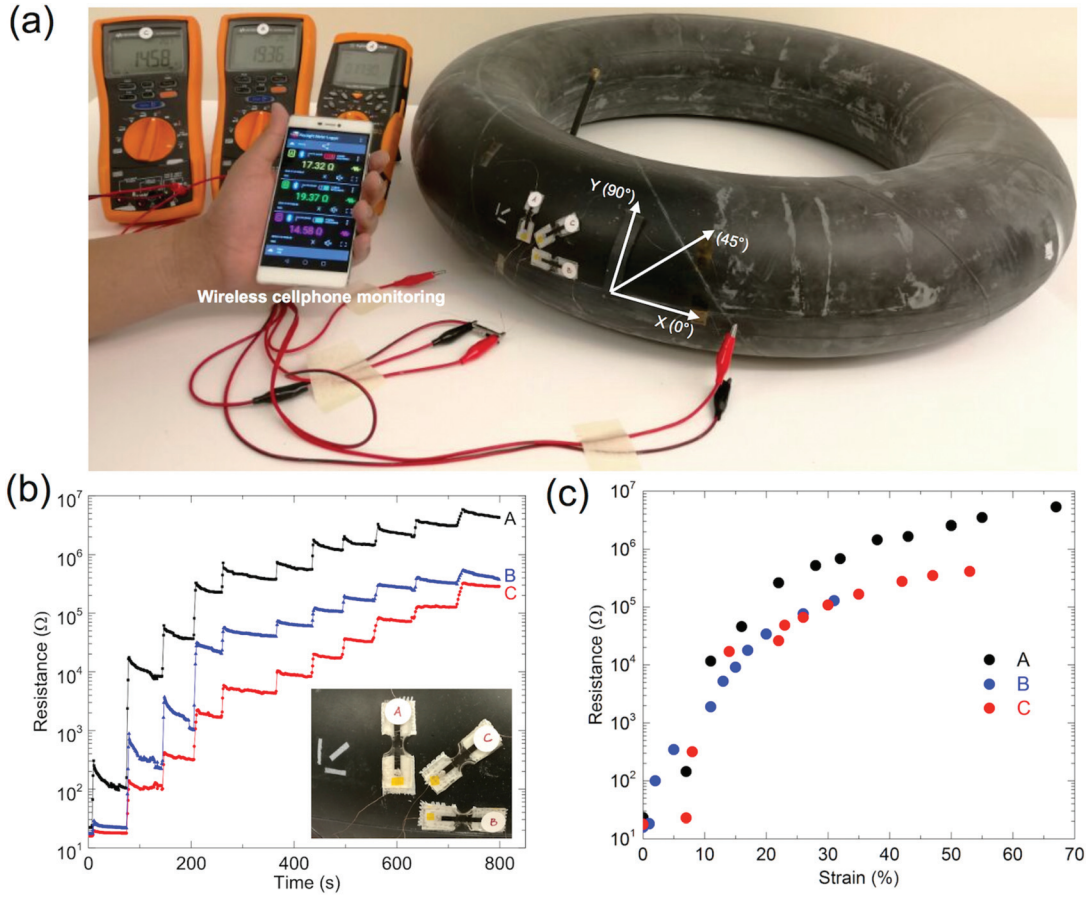

Fig. 5 Detection of the strain on a deformable surface. (a) A setup for measuring the strain variation during the inflation of a tire. 3 Channels of resistance data are collected on cellphone software through IR–bluetooth communication. (b) Resistance changes of the sensors under 11 steps of inflation of the tire. The inset in (b) shows the image of white marks for estimating the strain change in different directions and the 3 sensors attached to the tire, respectively. (c) The evolution of resistance with strain of the sensors at different locations.

cannot happen anymore between the fragments and the SWCNT-covered delaminated interface becomes the only possible conducting path. Electron tunneling is the dominant mechanism in the thin film as revealed by the frequency dependent impedance, and the phase data (Fig. 4c and d). Indeed, the dominant capacitive response at high frequency can be associated with the tunneling mechanism. This fact becomes clear when looking at the change in the phase angle, θ, at different strains. At higher strain ($\varepsilon > 20\%$), the capacitive part largely increases with frequency. This results from the disconnected SWCNT networks that act as capacitors instead of resistors.

3.4 Strain sensing application

We successfully demonstrate the capability of our sensors to detect strain on a deformable surface during the inflation process of a tire, as shown in Fig. 5. We attached three sensors (A, B, and C) to the tire at different angles of 90°, 0°, and 45°, respectively. The strain change of each sample was simultaneously measured by the length change of the white paint surface coating on the tire. We measured the output signal of the strain sensors when the tire was inflated by 11 incremental steps. Fig. 5a shows the resistance data of the sensors, collected through wireless communication between the multimeter and cellphone. Fig. 5b shows the response of the three sensors attached to the tire. Each expansion step of the tire was driven by increased air pressure and resulted in increased electrical resistance of the sensors. The evolution of the resistance with strain for the three sensors is shown in Fig. 5c. It clearly indicates that the sensors at 90° and 0° have the largest and smallest deformations, respectively. These results correspond to the different crack opening distance changes as shown in Fig. S8.† The cracks opened faster under the uniaxial strain of 90°, thus the resistance change became larger than 0° or 45°. Thus we confirmed that it is possible to differentiate the strain change at different locations, proving that our sensor can be used as a deformable mechanosensor for measuring the strain on complex expandable surfaces.

4. Conclusion

In summary, controlling the crack patterns in SWCNT paper through laser engraving and roll-to-roll pressing can help achieve high-performance strain sensors with high sensitivity, high stretchability, and high linearity. A sensitivity of 4.2×10^4 at a strain of 153% was achieved using a high crack-density SWCNT paper (3.3 mm^{-1}). The stretchability of such strain sensors could be tuned by varying the crack density. The controlled fragmentation process could potentially be applied to other nanomaterial-based structures for engineering the stretchability of a material while maintaining sensitivity. We believe that these techniques can inspire various designs of other sensitive and reversible strain-responsive materials with widespread applications.

Author contributions

J. Z. and G. L. proposed and supervised the research. Y. X. and J. Z. performed the experiments. Y. X., J. Z., X. X., and G. L. worked on the data analysis. J. Z., X. X., and G. L. wrote the manuscript.

Acknowledgements

The research reported in this paper was supported by funding from the King Abdullah University of Science and Technology (KAUST). The authors are grateful to the KAUST for its support.

References

1 M. Amjadi, K. Kyung, I. Park and M. Sitti, *Adv. Funct. Mater.*, 2016, **26**, 1678.
2 J. Park, I. You, S. Shin and U. Jeong, *ChemPhysChem*, 2015, **16**, 1155–1163.
3 A. Chortos, J. Liu and Z. A. Bao, *Nat. Mater.*, 2016, **15**, 937–950.
4 J. Zhou, E. Q. Li, R. Li, X. Xu, I. Aguilar Ventura, A. Moussawi, D. Anjum, M. N. Hedhili, D. Smilgies, G. Lubineau and S. T. Thoroddsen, *J. Mater. Chem. C*, 2015, **3**, 2528–2538.
5 J. Zhou, M. Mulle, Y. B. Zhang, X. Z. Xu, E. Q. Li, F. Han, S. T. Thoroddsen and G. Lubineau, *J. Mater. Chem. C*, 2016, **4**, 1238–1249.
6 H. Miura, Y. Fukuyama, T. Sunda, B. Lin, J. Zhou, J. Takizawa, A. Ohmori and M. Kimura, *Adv. Eng. Mater.*, 2014, **16**, 550–555.
7 J. Zhou, Y. Zhang, M. Mulle and G. Lubineau, *Meas. Sci. Technol.*, 2015, **26**, 085003.
8 Q. Cao and J. A. Rogers, *Adv. Mater.*, 2009, **21**, 29–53.
9 T. Yamada, Y. Hayamizu, Y. Yamamoto, Y. Yomogida, A. Izadi-Najafabadi, D. N. Futaba and K. Hata, *Nat. Nanotechnol.*, 2011, **6**, 296–301.
10 T. Q. Trung and N. Lee, *Adv. Mater.*, 2016, **28**, 4338–4372.
11 S. Zeng, D. Zhang, W. Huang, Z. Wang, S. D. Freire, X. Yu, A. T. Smith, E. Y. Huang, H. Nguon and L. Sun, *Nat. Commun.*, 2016, **7**, 11802.
12 J. Zhou, Y. Hu, X. Xu, F. Han and G. Lubineau, *ACS Appl. Mater. Interfaces*, 2017, **9**, 4835–4842.
13 J. Zhou, X. Xu, Y. Hu and G. Lubineau, *Nanoscale*, 2017, **9**, 604–612.
14 S. Gong, W. Schwalb, Y. W. Wang, Y. Chen, Y. Tang, J. Si, B. Shirinzadeh and W. L. Cheng, *Nat. Commun.*, 2014, **5**, 3132.
15 S. Gong, D. T. H. Lai, B. Su, K. J. Si, Z. Ma, L. W. Yap, P. Z. Guo and W. L. Cheng, *Adv. Electron. Mater.*, 2015, **1**, 1400063.
16 J. Ge, L. Sun, F. R. Zhang, Y. Zhang, L. A. Shi, H. Y. Zhao, H. W. Zhu, H. L. Jiang and S. H. Yu, *Adv. Mater.*, 2016, **28**, 722–728.

17 X. W. Wang, Z. P. Xiong, Z. Liu and T. Zhang, *Adv. Mater.*, 2015, **27**, 1370–1375.
18 J. Zhang, J. W. Liu, R. C. Zhuang, E. Mader, G. Heinrich and S. L. Gao, *Adv. Mater.*, 2011, **23**, 3392–3397.
19 H. H. Chou, A. Nguyen, A. Chortos, J. W. F. To, C. Lu, J. G. Mei, T. Kurosawa, W. G. Bae, J. B. H. Tok and Z. A. Bao, *Nat. Commun.*, 2015, **6**, DOI: 10.1038/ncomms9011.
20 H. Wang, B. W. Zhu, W. C. Jiang, Y. Yang, W. R. Leow, H. Wang and X. D. Chen, *Adv. Mater.*, 2014, **26**, 3638–3643.
21 D. J. Lipomi, *Adv. Mater.*, 2016, **28**, 4180–4183.
22 M. N. Saleh and G. Lubineau, *Sol. Energy Mater. Sol. Cells*, 2014, **130**, 199–207.
23 J. Lee, S. Kim, J. Lee, D. Yang, B. C. Park, S. Ryu and I. Park, *Nanoscale*, 2014, **6**, 11932–11939.
24 B. Park, J. Kim, D. Kang, C. Jeong, K. S. Kim, J. U. Kim, P. J. Yoo and T. Kim, *Adv. Mater.*, 2016, **28**, 8130–8137.
25 D. Kang, P. V. Pikhitsa, Y. W. Choi, C. Lee, S. S. Shin, L. F. Piao, B. Park, K. Y. Suh, T. I. Kim and M. Choi, *Nature*, 2014, **516**, 222–226.
26 T. Yang, X. Li, S. Lin, J. Lao, J. Shi, Z. Zhen, Z. Li and H. Zhu, *Mater. Horiz.*, 2016, **3**, 248–255.
27 Z. Y. Liu, D. P. Qi, P. Z. Guo, Y. Liu, B. W. Zhu, H. Yang, Y. Q. Liu, B. Li, C. G. Zhang, J. C. Yu, B. Liedberg and X. D. Chen, *Adv. Mater.*, 2015, **27**, 6230–6237.
28 M. Amjadi, M. Turan, C. P. Clementson and M. Sitti, *ACS Appl. Mater. Interfaces*, 2016, **8**, 5618–5626.
29 A. N. G. Parra-Vasquez, N. Behabtu, M. J. Green, C. L. Pint, C. C. Young, J. Schmidt, E. Kesselman, A. Goyal, P. M. Ajayan, Y. Cohen, Y. Talmon, R. H. Hauge and M. Pasquali, *ACS Nano*, 2010, **4**, 3969–3978.
30 Z. L. Li, P. Dharap, S. Nagarajaiah, E. V. Barrera and J. D. Kim, *Adv. Mater.*, 2004, **16**, 640–643.
31 D. J. Lipomi, M. Vosgueritchian, B. C. K. Tee, S. L. Hellstrom, J. A. Lee, C. H. Fox and Z. N. Bao, *Nat. Nanotechnol.*, 2011, **6**, 788–792.
32 W. Obitayo and T. Liu, *J. Sens.*, 2012, **2012**, 652438.
33 Y. R. Jeong, H. Park, S. W. Jin, S. Y. Hong, S. S. Lee and J. S. Ha, *Adv. Funct. Mater.*, 2015, **25**, 4228–4236.
34 Y. Cheng, R. Wang, J. Sun and L. Gao, *Adv. Mater.*, 2015, **27**, 7365–7371.
35 M. Amjadi, A. Pichitpajongkit, S. Lee, S. Ryu and I. Park, *ACS Nano*, 2014, **8**, 5154–5163.
36 Q. Liu, J. Chen, Y. Li and G. Shi, *ACS Nano*, 2016, **10**, 7901–7906.
37 S. Kang, A. R. Jones, J. S. Moore, S. R. White and N. R. Sottos, *Adv. Funct. Mater.*, 2014, **24**, 2947–2956.
38 K. K. Kim, S. Hong, H. M. Cho, J. Lee, Y. D. Suh, J. Ham and S. H. Ko, *Nano Lett.*, 2015, **15**, 5240–5247.